

Highly Efficient Hydroisomerization of *Endo*-Tetrahydrodicyclopentadiene to *Exo*-Tetrahydrodicyclopentadiene over Pt/HY

Wenke Wang, Jie Zhao, Dandan Jia, Zhaolin Fu, Enhui Xing, Zhongpeng Zhu, Rui Yan, Zhiping Tao,* Yibin Luo, and Xingtian Shu



Cite This: *ACS Omega* 2021, 6, 17173–17182

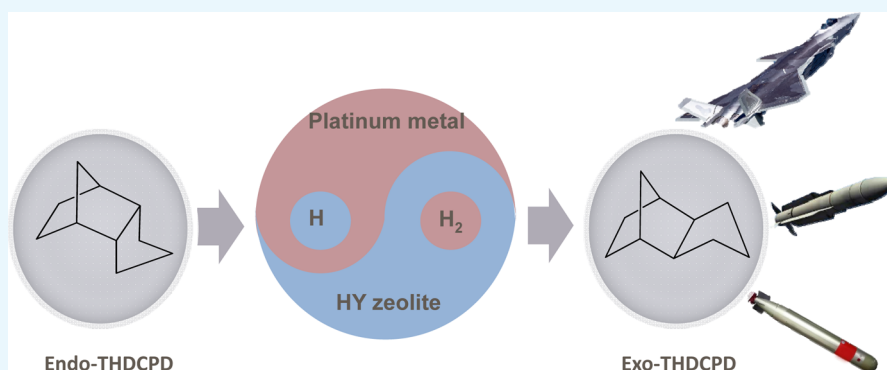


Read Online

ACCESS |

Metrics & More

Article Recommendations



ABSTRACT: The fast deactivation caused by serious formation of coke is a major challenge in catalytic isomerization of *endo*-tetrahydrodicyclopentadiene (*endo*-THDCPD) into *exo*-tetrahydrodicyclopentadiene (*exo*-THDCPD) over the HY zeolite. In order to suppress the coke formation for the isomerization process, the conventional HY zeolite was modified with Pt at 0.3 wt %. Then, the hydroisomerization of *endo*-THDCPD into *exo*-THDCPD was evaluated over a fixed-bed reactor. The catalytic stability of Pt/HY was greatly enhanced in comparison to that of the HY zeolite. The Pt/HY catalyst provided 97% *endo*-THDCPD conversion and 96% selectivity for *exo*-THDCPD without deactivation after 100 h. Moreover, the formation mechanism of coke on the HY zeolite during the isomerization process was proposed based on the results of the coke analysis. It was indicated that the coke was generated from the oligomerization and condensation of olefin species, which originated from the β -scission reaction or hydride transfer reaction of intermediates. The lower coke formation over Pt/HY was attributed to the lower amount of coke precursors, which could be hydrogenated by activated H_2 over Pt sites. Therefore, Pt on Pt/HY and H_2 were two crucial factors in efficiently enhancing the catalytic stability of the HY zeolite for this isomerization reaction.

1. INTRODUCTION

Due to the low toxicity, high energy density (39.6 MJ L^{-1}), suitable flash point ($55 \text{ }^\circ\text{C}$), low freezing point ($-79 \text{ }^\circ\text{C}$), and satisfactory long-term storage stability, *exo*-tetrahydrodicyclopentadiene (*exo*-THDCPD; IUPAC name, *exo*-tricyclo[5.2.1.0^{2,6}]decane) is the main component of the high-energy-density liquid fuel referred to as JP-10, which is a commonly used jet fuel for small missiles.^{1–3} In addition, *exo*-THDCPD can be utilized as a diluent for other high-energy-density fuels like JP-9, RJ-5, and RF-1 in various missiles/aircraft.^{4–6} Moreover, *exo*-THDCPD is a high-value fine chemical, which could be used in surfactants, dyes, and so on.^{7,8}

Exo-THDCPD was usually synthesized by isomerizing its *endo*-isomer (*endo*-THDCPD) in the presence of strong acid catalysts, which included homogeneous and heterogeneous

catalysts. In previous studies, highly corrosive sulfuric acid was used to catalyze this reaction.^{9,10} Since the 1960s, *exo*-THDCPD was commercially produced from *endo*-THDCPD with the aluminum trichloride (AlCl_3) catalyst in a batch reactor, which suffered from several drawbacks, such as catalyst non-recyclability, environmental problems, and purification problems.¹¹ Although, the immobilization of AlCl_3 on inorganic solid supports brought the advantages of easy

Received: January 20, 2021

Accepted: March 23, 2021

Published: June 30, 2021



separation, the ease of deactivation and environmental pollution limited its application at an industrial scale.¹² The chloroaluminate-based ionic liquid (IL) catalyst was a potential substitute for AlCl_3 due to the adjustable acidity. However, the problems of separation and recycling are still hard to be solved because of the presence of a homogeneous catalytic process. Besides, AlCl_3 -based IL catalysts are also toxic and could cause environmental pollution.^{13,14} Recent work concerning the use of zeolite catalysts in place of AlCl_3 has resolved the separation and environmental problems. For example, Xing et al. reported a green synthetic route for the isomerization reaction catalyzed by acidic Y zeolites with different cations, and HY showed an optimum catalytic activity with 90% conversion of *endo*-THDCPD and 95% selectivity for *exo*-THDCPD at 195 °C.¹⁵ Moreover, Sun and Li discussed the effect of temperature and reaction time on *endo*-THDCPD isomerization in the gas phase (flow system) by using the H-USY zeolite.¹⁶ Li et al. investigated a synthetic route for preparing *exo*-THDCPD from lignocellulose, and the catalyst used in the isomerization of *endo*-THDCPD is the LaY zeolite. The overall carbon yield of *exo*-THDCPD was 65% under the optimized conditions.¹⁷ Although the acidic Y zeolites showed a good catalytic activity, the easy deactivation caused by rapid formation of coke deposited on the zeolite limited its application.^{15,16} Therefore, it is necessary to suppress the formation of coke to improve the catalytic stability of the Y zeolite for continuous isomerization of *endo*-THDCPD to *exo*-THDCPD over a fixed-bed reactor.

Presently, systematic studies are not yet published on the composition and properties of coke compounds deposited on the catalyst for the reaction. For instance, Wang et al. first reported a one-step catalytic flow-phase hydrogenation–isomerization of dicyclopentadiene (DCPD) to *exo*-THDCPD over a fixed-bed reactor. Therein, the $\text{Ni}/\gamma\text{-Al}_2\text{O}_3$ catalyst was used for the hydrogenation of DCPD, and the $\text{Ni}/\text{H}\beta$ catalyst was used for the isomerization of *endo*-THDCPD. This process provided 100% DCPD conversion and 70% selectivity for *exo*-THDCPD without obvious deactivation over 200 h.¹⁸ However, in this study, Ni/HY showed poor activity with 100% DCPD conversion and only 6.8% selectivity for *exo*-THDCPD. Although $\text{Ni}/\text{H}\beta$ provided the optimum activity, the byproducts formed on $\text{Ni}/\text{H}\beta$ were not systematically analyzed. It is not yet clear whether the Ni on $\text{Ni}/\text{H}\beta$ could actually be beneficial to suppress the formation of coke and enhance the stability of the process. In general, for the isomerization of many alkanes catalyzed by acid zeolites, the unsaturated species which lead to the rapid formation of coke are intermediates or products formed during the isomerization process.^{19,20} Under a H_2 atmosphere, these coke precursors could be converted to saturated hydrocarbons catalyzed by metallic sites for hydrogenation and then removed, resulting in suppressing the coke formation.^{21–27}

To the best of our knowledge, there are rare studies investigating the hydroisomerization of *endo*-THDCPD to *exo*-THDCPD catalyzed by the Pt/HY zeolite catalysts over a fixed-bed reactor. We report here the first study about the interactive effect of H_2 and Pt on the coking behaviors during the hydroisomerization of *endo*-THDCPD to *exo*-THDCPD over Pt/HY , aiming to suppress the coke formation and enhance the catalytic stability of the catalyst.

2. EXPERIMENTAL SECTION

2.1. Materials. *Endo*-THDCPD (>99 wt %) was purchased from Hangzhou Yangli Petrochemical Co. Ltd., and used

without further purification. Methyl cyclohexane was supplied by Aladdin Co. Ltd. and utilized as the solvent for the isomerization of *endo*-THDCPD. HY ($\text{SiO}_2/\text{Al}_2\text{O}_3 = 5.2$) was provided by the Research Institute of Petroleum Processing.

2.2. Catalyst Preparation. The 0.3 wt % Pt/HY catalyst was prepared via incipient wetness impregnation of HY zeolite powder with $\text{Pt}(\text{NH}_3)_4\text{Cl}_2$ as the metal precursor and H_2O as the solvent, and the pH for the aqueous solution of $\text{Pt}(\text{NH}_3)_4\text{Cl}_2$ was 6.7. After impregnation and drying in an oven at 80 °C overnight, the sample $\text{Pt}/\text{HY}\text{-BQ}$ was obtained and then precalcined at 450 °C for 3 h to generate Pt/HY .

2.3. Characterization. The powder X-ray diffraction (XRD) patterns of catalysts were taken using an EMPYREAN X-ray diffractometer (PANalytical Japan) in the 2θ range of 5–70° with $\text{Cu K}\alpha$ radiation at 35 kV and 35 mA. The Brunauer–Emmett–Teller (BET) specific surface area and pore size of the catalysts were measured by N_2 adsorption–desorption at 77 K using a Quantachrome AS-3. Transmission electron microscopy (TEM) analysis was performed on a JEM-2100 (200 kV) EX electron microscope. The fourier transform infrared spectra of pyridine adsorbed on the catalyst were recorded on a NICOLET 6700 spectrometer.

Thermogravimetric analysis (TGA) was exploited to determine the amounts and characteristics of the coke formed on the spent catalysts. TGA measurements were conducted using a STA 449 F5 thermogravimetric analyzer at a heating rate of 5 °C min^{-1} from 50 to 800 °C under a continuous flow of 20% oxygen in helium. To determine the components of coke present on the coked samples, the coked samples were dissolved in 40% hydrofluoric acid. Then, the coke was extracted with methylene chloride, and the resulting mixture was concentrated and subsequently analyzed by gas chromatography and mass spectrometry (GC–MS) and apex-Qe 9.4T fourier transform ion cyclotron resonance mass spectrometry (FT-ICR MS) with Agilent atmospheric pressure photoionization.

2.4. Catalytic Experiments. In the first experiment, the liquid-phase isomerization of *endo*-THDCPD to *exo*-THDCPD catalyzed by the HY zeolite was performed over a fixed-bed reactor at 150 °C, 0.5 MPa with a weight hourly space velocity (WHSV) = 2.0 h^{-1} . The HY zeolite was activated for 3 h at 450 °C prior to the run. The *endo*-THDCPD dissolved in methyl cyclohexane was placed in a liquid tank and was injected into the reactor and passed over the catalyst. Product analysis was carried out by using an Agilent 7890B gas chromatograph (Agilent Technologies) equipped with a HP-5 capillary column (0.32 mm \times 0.50 μm \times 30 m) and a flame ionization detector with a vaporizer temperature of 250 °C, a column temperature of 50 °C, and a detector temperature of 300 °C.

In comparison, the second isomerization experiment of *endo*-THDCPD was carried out in a continuous flow fixed-bed reactor operated at 150 °C, WHSV = 2.0 h^{-1} , H_2 or N_2 pressure = 0.5 MPa, and H_2 or N_2/endo -THDCPD (mol/mol) = 30. In each experiment, the catalyst (20–40 mesh, total mass equal to 5 g) was loaded in the constant-temperature zone and reduced under flowing H_2 at 450 °C for 3 h prior to each run. After each run, the catalyst bed was purged with N_2 flow (250 mL min^{-1}) at 100 °C for 3 h in order to eliminate the components remaining on the catalysts. HY and Pt/HY after reaction operation for 8 h under N_2 or H_2 atmosphere were denoted as $\text{HY}\text{-N}_2\text{-8h}$, $\text{HY}\text{-H}_2\text{-8h}$, $\text{Pt}/\text{HY}\text{-N}_2\text{-8h}$, and $\text{Pt}/\text{HY}\text{-H}_2\text{-8h}$, respectively. Pt/HY after reaction operation for 150 h

under a H₂ atmosphere was denoted as Pt/HY-H₂-150h. The product selectivity was calculated according to the following equation:

$$\text{selectivity} = \left\{ \frac{\text{mass of certain product}}{\text{mass of endo-THDCPD feed} - \text{mass of endo-THDCPD in the product}} \right\} \times 100\%$$

3. RESULTS AND DISCUSSION

3.1. Catalyst Characterization. As shown in Figure 1, it could be seen that both HY and Pt/HY showed the typical

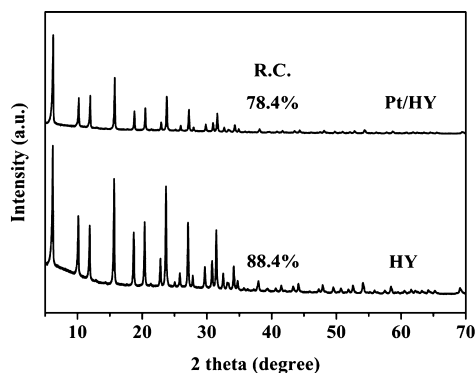


Figure 1. XRD patterns of HY and Pt/HY.

topological structure of zeolite Y in the 2θ region of 4–40°. No significant change was observed after the loading of Pt. However, the relative crystallinity of Pt/HY slightly decreased to 78.4% compared with HY (88.4%), indicating that the pore structure of HY was destroyed to a certain extent after loading of Pt. The characteristic peak of Pt was not observed in Pt/HY, which could be attributed to the low loading and the high dispersion of Pt clusters on HY.²⁹ Combining the TEM images in Figure 2a,b, it could be observed that the Pt clusters were uniformly dispersed on HY, with the particle size ranging 1.5–3.0 nm. As shown in Figure 3a, the isotherm of HY was assigned to a combination of type I and type IV in IUPAC classification, suggesting the microporosity of the materials containing narrow cylindrical pores and mesopores.³⁰ The N₂ adsorption–desorption isotherm of Pt/HY was similar to that of the HY zeolite. The pore size distributions were calculated from the adsorption isotherm by the Barrett–Joyner–Halenda method, as shown in Figure 3b. The mean pore diameter of Pt/HY was larger than that of the HY zeolite. The textural properties of HY and Pt/HY assessed from the N₂ adsorption–desorption isotherm are summarized in Table 1. For the Pt/

HY catalyst, there was no obvious change in the mesopore volume, while both the surface area and micropore volume got slightly decreased. The differences between Pt/HY and HY were probably assigned to the destruction of the pore structure due to calcination during the process of Pt loading.

In order to confirm the change in the coordination environment for the aluminum in the samples, the ²⁷Al magic-angle spinning (MAS) NMR spectra of HY, Pt/HY-BQ, and Pt/HY were recorded and are shown in Figure 4. In all spectra of the samples, there were two signals with chemical shifts at 60 and 0 ppm corresponding to the tetrahedral aluminum species in the framework and octahedral extra-framework aluminum, respectively. Pt/HY-BQ showed similar intensity of signals at 60 and 0 ppm to the HY zeolite, revealing that no obvious destruction of the chemical surroundings of framework aluminum generated during the impregnation process of HY with the solution of Pt(NH₃)₄Cl₂. For the Pt/HY sample, the signal at 0 ppm for the octahedral form of the extra-framework Al was stronger than that of HY and Pt/HY-BQ, implying that some amount of tetrahedral aluminum was transformed to octahedral extra-framework aluminum during the process of calcination of Pt/HY-BQ to Pt/HY. Thus, the high-temperature calcination step was responsible for the presence of extra-framework aluminum sites and destruction of the pore structure of Pt/HY.

The acidity of the samples, which was determined by IR-pyridine experiments, is presented in Table 2. Both the HY zeolite and Pt/HY possessed weak and strong acid sites, and they exhibited both types of Brønsted and Lewis acid sites. It was observed that Pt/HY possessed fewer Brønsted acid sites compared with HY, which was probably attributed to the slight modification in the acid property during the calcination process.³⁰ However, Pt/HY showed a higher number of Lewis acid sites than the HY zeolite. This result could be ascribed to new Lewis acid sites generated from the modification of the zeolite skeleton structure caused by calcination.

3.2. Catalytic Performances. The liquid-phase isomerization of *endo*-THDCPD into *exo*-THDCPD was tested over the HY zeolite. The *endo*-THDCPD conversion and selectivity for *exo*-THDCPD results are shown in Figure 5a. From the results, it was clearly observed that the *endo*-THDCPD conversion decreased from 97.6 to 12.2% after 8 h for the isomerization process. This result indicated that the HY zeolite was easily deactivated for the reaction, which was not feasible for industrial applications. In comparison, the *endo*-THDCPD conversion and selectivity for *exo*-THDCPD over Pt/HY in the presence of H₂ are shown in Figure 5b. This process displayed better catalytic stability and provided 98% conversion of *endo*-THDCPD and over 92% selectivity of *exo*-THDCPD after 8 h,

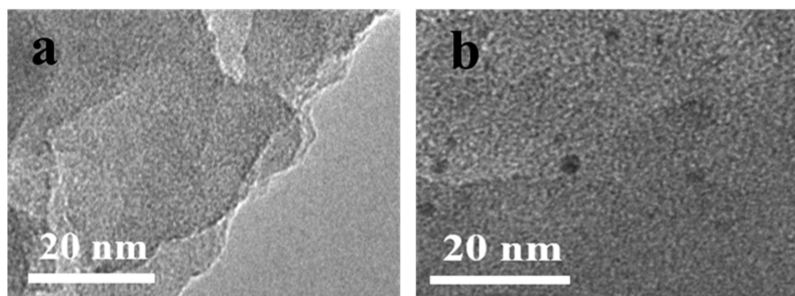


Figure 2. TEM images of (a) HY and (b) Pt/HY.

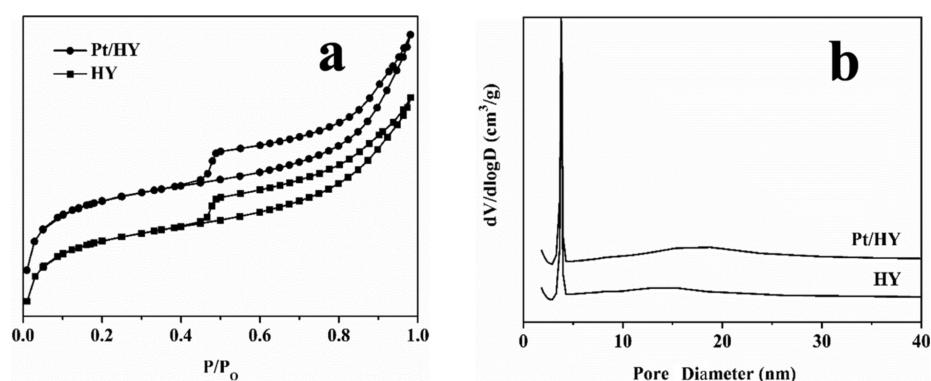


Figure 3. (a) N_2 adsorption–desorption curve of HY and Pt/HY and (b) pore size distribution of HY and Pt/HY.

Table 1. Textural Properties of HY and Pt/HY

catalyst	S_{BET} (m^2/g)	S_{micro} (m^2/g)	S_{meso} (m^2/g)	V_{total} (cm^3/g)	V_{micro} (cm^3/g)	V_{meso} (cm^3/g)
HY	652	628	24	0.345	0.290	0.055
Pt/HY	604	581	23	0.323	0.269	0.054

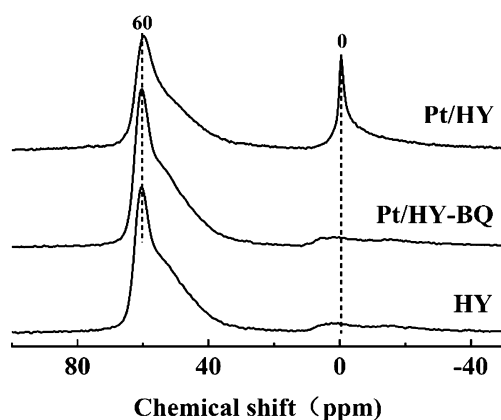


Figure 4. ^{27}Al MAS NMR spectra of HY, Pt/HY-BQ, and Pt/HY.

indicating that the presence of Pt and H_2 probably accounted for enhancing the catalytic stability of HY.

To confirm the functions of Pt and H_2 for the activity and catalytic stability of HY, the catalytic isomerization of *endo*-THDCPD was carried out over HY and Pt/HY in the presence of H_2 or N_2 . The isomerization process was usually accompanied by the formation of adamantane and ring-opening products.^{11,16} The yields of *exo*-THDCPD and other byproducts at first hour are provided in Figure 6. It could be found that both HY and Pt/HY exhibited similar approximately 98% conversion regardless of a H_2 or N_2 atmosphere. Xing's work showed that Brønsted acid site strength is more important than acidity numbers for the isomerization of *endo*-THDCPD to *exo*-THDCPD.¹⁵ Besides, the extra-framework aluminum as Lewis acid sites has a positive effect on increasing the acid strength of some Brønsted acid sites through interaction with the zeolite framework. It could be observed

Table 2. Acid Properties of HY and Pt/HY

catalyst	200 °C			350 °C		
	Brønsted acid ($\mu\text{mol}/\text{g}$)	Lewis acid ($\mu\text{mol}/\text{g}$)	B/L	Brønsted acid ($\mu\text{mol}/\text{g}$)	Lewis acid ($\mu\text{mol}/\text{g}$)	B/L
HY	628	22	28.55	583	12	48.58
Pt/HY	486	136	3.57	414	90	4.60

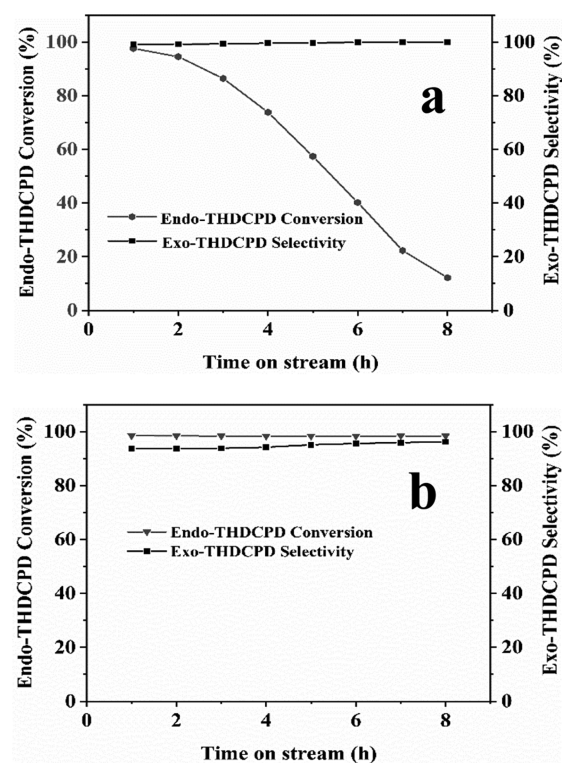


Figure 5. (a) Catalytic activity over the HY zeolite. Reaction conditions: $T = 150\text{ }^\circ\text{C}$, $P = 0.5\text{ MPa}$, $\text{WHSV} = 2\text{ h}^{-1}$. (b) Catalytic activity over Pt/HY zeolite. Reaction conditions: $T = 150\text{ }^\circ\text{C}$, $P = 0.5\text{ MPa}$, $\text{WHSV} = 2\text{ h}^{-1}$, $\text{H}_2/\text{endo-THDCPD}$ (mol/mol) = 30.

that Pt and H_2 had no obvious effect on the initial catalytic activity of HY.³¹ For the HY zeolite, the results shown in Figure 6 demonstrated that H_2 was beneficial to the formation of ring-opening products, while it contributed little to the production of adamantane. For Pt/HY, it could be observed that Pt/HY possessed a similar selectivity of *exo*-THDCPD to that over HY in the first hour under the N_2 atmosphere. However, the initial selectivity of ring-opening products over Pt/HY was higher than that of HY under the N_2 atmosphere,

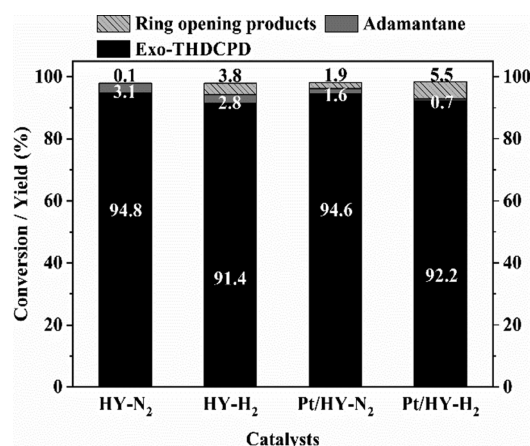


Figure 6. Catalytic activity of the catalysts during the isomerization of *endo*-THDCPD in a H₂ or N₂ atmosphere at the first hour. Reaction conditions: $T = 150\text{ }^{\circ}\text{C}$, $P = 0.5\text{ MPa}$, $\text{WHSV} = 2\text{ h}^{-1}$, H₂ or N₂/*endo*-THDCPD (mol/mol) = 30.

suggesting that Pt could promote the formation of ring-opening products during the isomerization of *endo*-THDCPD. Moreover, the initial selectivity of adamantane over Pt/HY was lower than that over HY in the presence of N₂. This change was ascribed to a decrease in the number of the strong Brønsted acid sites on Pt/HY as the existing study showed that strong Brønsted acid sites on HY were beneficial to the formation of adamantane.³² Under the H₂ atmosphere, Pt/HY showed an obvious higher initial yield of ring-opening products than that under the N₂ atmosphere, indicating that Pt and H₂ could directly promote the formation of ring-opening products for the reaction.^{33–35} Although the presence of Pt and H₂ could decrease the selectivity of *endo*-THDCPD, it would play a key role in enhancing the catalytic stability of the HY zeolite. As shown in Figure 7, Pt/HY and HY displayed different catalytic lifespans at a H₂ or N₂ pressure of 0.5 MPa. For HY in the N₂ atmosphere, the *endo*-THDCPD conversion dramatically decreased to 56% after only 8 h. Besides, it was observed that H₂ had no desired effect on improving the catalytic stability of the HY zeolite. Similar to the HY zeolite, Pt/HY was easily deactivated after 8 h at a N₂ pressure of 0.5 MPa. In contrast, the catalytic lifespan of Pt/HY was greatly enhanced under a H₂ pressure of 0.5 MPa. The *endo*-THDCPD conversion of the Pt/HY still attained 97% with a selectivity of 96% for *exo*-THDCPD after 100 h. As discussed above, the presence of Pt and H₂ probably was favorable for the formation

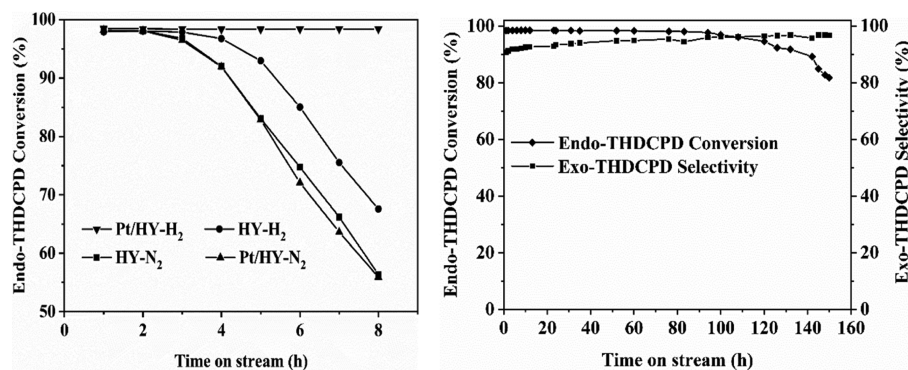


Figure 7. Catalytic activity of the catalysts during the isomerization of *endo*-THDCPD. Reaction conditions: $T = 150\text{ }^{\circ}\text{C}$, $P = 0.5\text{ MPa}$, $\text{WHSV} = 2\text{ h}^{-1}$ and H₂ or N₂/*endo*-THDCPD (mol/mol) = 30.

of the ring-opening byproducts. However, the presence of H₂ and Pt was essential to enhance the catalytic stability of the HY zeolite during the isomerization of *endo*-THDCPD.

3.3. Characterization of Cokes Deposited on the Catalysts. It has been known that coke deposition is responsible for zeolite catalyst deactivation for the isomerization of *endo*-THDCPD, while reports about the details of coking behaviors are still rare.¹⁵ The coked samples were utilized for coke analysis to understand the deactivation behavior and evaluate the effect of Pt and H₂ on depressing the formation of coke over the HY zeolite. The content of coke was measured by TGA in air, as shown in Figure 8. The mass

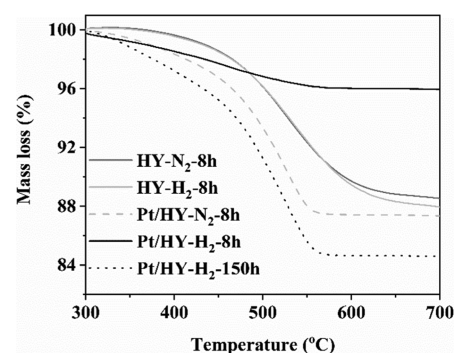


Figure 8. TGA curves of the catalysts after stability test.

loss of the catalysts below 300 °C was mainly assigned to the water loss and physically adsorbed compounds, which was not considered in calculations.¹⁸ All the coked samples were normalized to the weight at 300 °C. The two weight loss regions in the temperature range of 300–500 and 500–750 °C were associated to the oxidation of soft coke and hard coke.^{18,36,37} The total coke content of HY-N₂-8h, HY-H₂-8h, Pt/HY-N₂-8h, and Pt/HY-H₂-8h was 11.55, 12.14, 12.60, and 3.81 wt %, respectively. A large amount of coke was accumulated on the HY zeolite after only 8 h, accompanied by the rapid deactivation of the catalysts whether under the H₂ or N₂ atmosphere, showing that H₂ or N₂ had no effect on suppressing the formation of coke on the HY zeolite. Similar to the HY zeolite, serious coke formation occurred quickly over Pt/HY under the N₂ atmosphere after only 8 h. However, the content of total coke for Pt/HY-H₂-8h was 3.81 wt %. The total coke content over Pt/HY was only 15.33 wt % when the reaction time was prolonged to 150 h under the H₂ atmosphere. This result confirmed that H₂ and Pt were

superior for suppressing the coking formation, resulting in enhancing the catalytic stability of the HY zeolite. However, coke would be generated slowly on Pt/HY during the hydroisomerization of *endo*-THDCPD. Thus, the deactivation of Pt/HY after 100 h could be reasonably attributed to the channel blocking and loss of acidic sites over Pt/HY by coke formation during the hydroisomerization of *endo*-THDCPD. It was also seen that the hard coke content of HY-N₂-8h and HY-H₂-8h was 7.59 and 8.19 wt %, respectively, and the hard coke content of Pt/HY-N₂-8h, Pt/HY-H₂-8h, and Pt/HY-H₂-150h was 5.97, 0.88, and 6.60 wt %, respectively. Compared with HY-N₂-8h, the content of hard coke for Pt/HY-N₂-8h decreased, which could be attributed to the decrease in the number of the strong Brønsted acid sites of Pt/HY. Moreover, Pt/HY-H₂-8h showed lower hard coke content than that of HY-H₂-8h and Pt/HY-N₂-8h. This result could be ascribed to the inhibition of hard coke formation in the presence of Pt and H₂. Combining the results in Figure 6, it was evident that the coke formation and hard coke could be suppressed over Pt/HY under the H₂ atmosphere, resulting in enhancing the catalytic stability of HY.

In order to further study how Pt and H₂ work in inhibiting coke formation over Pt/HY in the isomerization process, it is necessary to characterize the composition of soft coke and hard coke on the coked samples. These coked samples were dissolved in 40% hydrofluoric acid, followed by the soluble coke being extracted with dichloromethane for GC–MS analysis.^{38,39} The GC–MS analysis results are shown in Table 3. For the spent HY-N₂-8h, HY-H₂-8h, Pt/HY-N₂-8h,

Table 3. Content of Low-Boiling Soluble Coke Species Deposited on the Coked Samples

sample	soft coke content (%)	molecular weight	formula	content (%)
HY-N ₂ -8h	3.96	270	C ₂₀ H ₃₀	2.25
		272	C ₂₀ H ₃₂	1.71
HY-H ₂ -8h	3.95	270	C ₂₀ H ₃₀	2.17
		272	C ₂₀ H ₃₂	1.78
Pt/HY-N ₂ -8h	6.63	270	C ₂₀ H ₃₀	4.41
		272	C ₂₀ H ₃₂	2.22
Pt/HY-H ₂ -8h	2.93	270	C ₂₀ H ₃₀	2.93
		272	C ₂₀ H ₃₂	0.00
Pt/HY-H ₂ -150h	8.73	270	C ₂₀ H ₃₀	5.33
		272	C ₂₀ H ₃₂	3.40

Pt/HY-H₂-8h, and Pt/HY-N₂-150h, there were almost no solid residues (insoluble coke) after the extraction of soluble coke from these coked samples with dichloromethane. The GC–MS analysis results showed that the soluble coke were complex mixtures. The general formula of the soluble coke component with low boiling point was usually assigned to soft coke.³⁸ It could be observed that the low-boiling soluble coke was primarily compounds with 20 carbon atoms and the soft coke was composed of two coke components with a molecular weight of 270 and 272. The formation of C₂₀ coke components could be explained by the dimerization of the reaction intermediates or byproducts. Besides, the coke components with a molecular weight of 272 should be dimers of reactants (molecular weight = 136). Furthermore, these coked samples showed different contents of these two coke components. The content of coke components with a molecular weight of 270 deposited on Pt/HY-H₂-8h and Pt/HY-H₂-150h was 2.93 and

5.33 wt %, respectively, and the content of coke components with a molecular weight of 272 was 0 and 3.40 wt %, respectively. The content of soluble coke components with a molecular weight of 272 on Pt/HY-N₂-8h and HY-H₂-8h was higher than that of Pt/HY-H₂-8h. Moreover, Pt/HY-H₂-150h showed a higher content of coke components with a molecular weight of 272 than Pt/HY-H₂-8h. These results indicated that the formation of the coke components with a molecular weight of 272 should play a relatively main role in the deactivation of the HY zeolite. Therefore, it was verified that the presence of Pt and H₂ could greatly affect the composition of soft coke during the hydroisomerization of *endo*-THDCPD.

Furthermore, the GC–MS analysis routinely used for low-boiling fractions is inadequate for the characterization of high-boiling materials due to their low volatility and compositional complexity. It could be known that FT-ICR MS has been widely used to characterize crude oil at the molecular level due to its superior ability.^{40,41} FT-ICR MS analysis of soluble coke was utilized to definitely characterize the hard coke components with higher molecular weight in the soluble carbonaceous species. Figure 9 showed the broadband mass

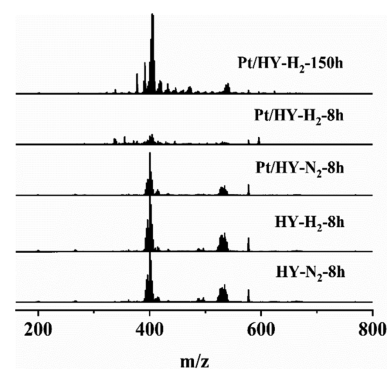


Figure 9. Broadband positive-ion APPI FT-ICR mass spectra for the soluble coke components deposited on deactivated catalysts.

spectrum for coke components deposited on the five used catalysts. The higher-molecular-weight coke species were more compositionally complex. HY-N₂-8h, HY-H₂-8h, and Pt/HY-N₂-8h presented similar mass distributions. The higher-molecular-weight soluble coke ranged from *m/z* 380 to 580 with the mass distribution centered at *m/z* 400 and 534. For Pt/HY-H₂-8h, the mass distribution of soluble coke ranged from *m/z* 300 to 600, and the most abundant was at *m/z* 415. Compared with Pt/HY-H₂-8h, Pt/HY-H₂-150h showed a broader mass distribution ranging from *m/z* 300 to 700, accompanied by the center of the molecular weight distribution shifted to a higher *m/z* value.

The trapped soluble coke species deposited on the coked samples were extracted with dichloromethane for GC–MS analysis. The carbon number distribution and bubble diagram of double-bond equivalents (DBEs) of coke components with a higher molecular weight could not be obtained from the results of GC–MS analysis. The FT-ICR MS analysis results showed isoabundance-contoured plots of DBEs versus the carbon number for the soluble coke of coked samples, as it was shown in Figure 10. The DBE was taken as the ordinate, the carbon number was taken as the *x*-coordinate, and the bubble area size represented the relative content of the substance. The hydrocarbon class for HY-H₂-8h had carbon number distributions between C₂₀ to C₆₀, and the higher abundance

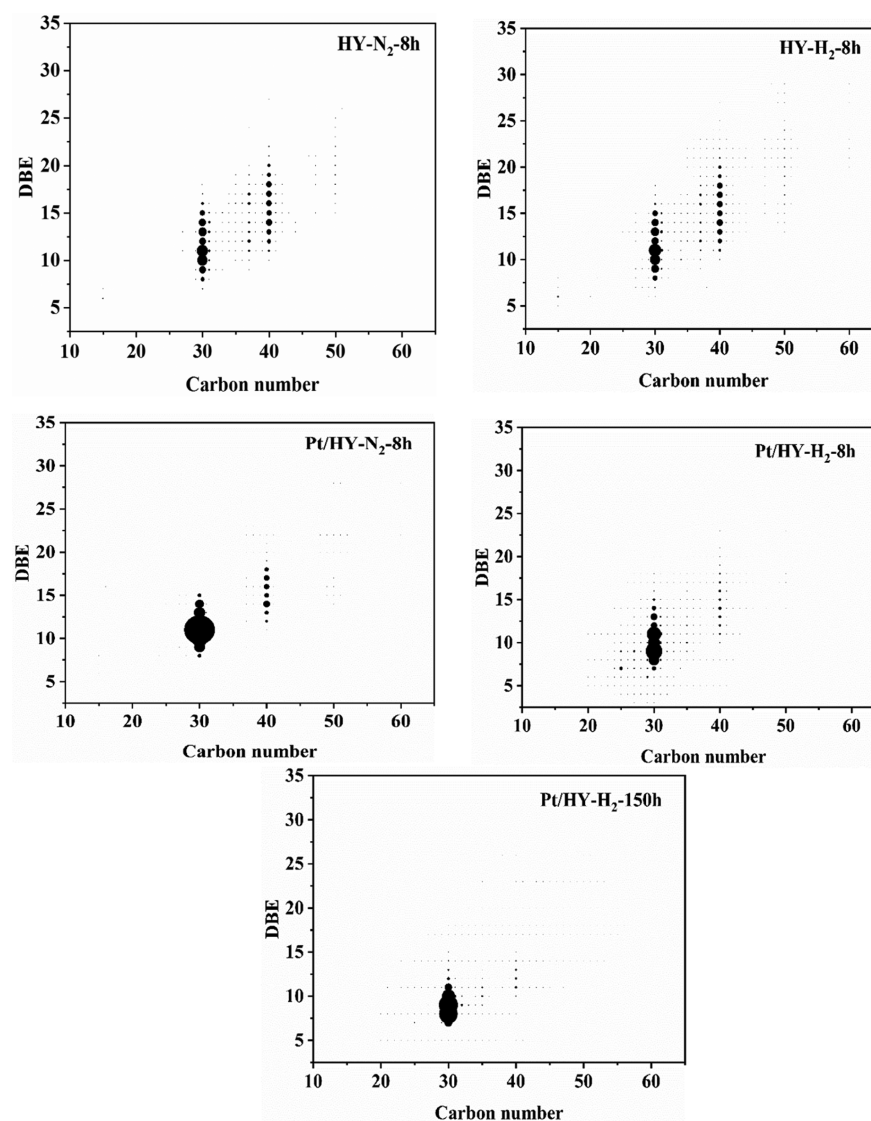


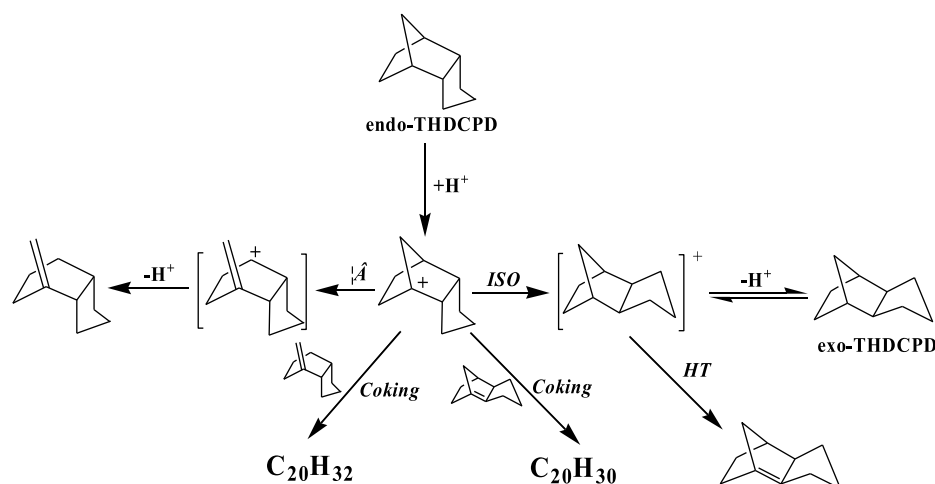
Figure 10. Isoabundance-contoured plots of DBEs vs carbon number for the coke components deposited on used catalysts.

was at C_{30} and C_{40} . HY- N_2 -8h did not show any significant difference in the carbon number distributions compared with HY- H_2 -8h, and the soluble coke were of a wide carbon number range (C_{20} – C_{60}). Pt/HY- H_2 -8h had the carbon number distribution from C_{20} to C_{50} with the highest abundance at C_{30} . Besides, Pt/HY- H_2 -150h showed similar results to Pt/HY- H_2 -8h. As shown in Figure 10, the DBE values of soluble carbonaceous species deposited on Pt/HY- H_2 -8h and Pt/HY- H_2 -150h were significantly decreased compared to those of HY- N_2 -8h, HY- H_2 -8h, and Pt/HY- N_2 -8h. For example, HY- H_2 -8h had a highest relative abundance at C_{30} with DBE values ranging from 8 to 15, whereas Pt/HY- H_2 -150h had the highest abundance at C_{30} with a decreased DBE from 7 to 13. Combining the DBE distribution and carbon number distribution of soluble coke, it could be concluded that the coke deposited on these used catalysts was mainly composed of the trimerization and tetramerization products from reaction intermediates. The high-molecular-weight coke components with low DBE were more likely to be formed on HY- N_2 -8h, HY- H_2 -8h, and Pt/HY- N_2 -8h than on Pt/HY- H_2 -8h and Pt/HY- H_2 -150h, which was consistent with the TGA results, implying that the formation of high-molecular-weight coke

components with high unsaturation could be suppressed on Pt/HY in the presence of H_2 .

Generally, the coke blocked inside the pores or deposited on the surface of zeolites is responsible for their deactivation during the serious processes of refining and petrochemicals. As reported, the critical dimension of *endo*-THDCPD was 0.67×0.65 nm, and the critical dimension of *exo*-THDCPD was 0.67×0.60 nm.⁴² The HY zeolite could provide sufficient space for the isomerization of *endo*-THDCPD to *exo*-THDCPD, while a pore diffusion limitation would generate in this situation when HY was used to catalyze the oligomerization of cyclopentadiene to tricyclopentadiene.⁴³ Thus, the coke components probably had a bigger critical diameter than the pore size of the HY zeolite.⁴⁴ Therefore, the supercages of HY could be blocked by the coke components, resulting in the rapid deactivation of the HY zeolite. Besides, their retention in the HY zeolite pores was also associated with low volatility, as the soluble coke components had a carbon number range (C_{20} – C_{60}) and their boiling points were much higher than the isomerization temperature (150 °C). Therefore, the rapid deactivation of catalysts was attributed to the coke components deposited on the HY zeolite blocking the access of *endo*-

Scheme 1. Proposed Mechanism for the Formation of Coke over the Pt/HY Bifunctional Catalyst during the Hydroisomerization of *Endo*-THDCPD^a



^aISO, isomerization; β , β -scission; HT, hydride transfer.

THDCPD to the acid sites in the supercages or covering the acid sites. The presence of Pt and H₂ was beneficial to enhance the catalytic stability of the HY zeolite by depressing the formation of coke and restricting the oligomerization degree of coke precursors, as the coke precursors could be hydrogenated to saturated hydrocarbons by H₂ over Pt sites and removed.^{45–48}

3.4. Mechanism of Coke Formation. The mechanism of coke formation was discussed on the basis of the above-mentioned characterization results. As mentioned before, it was most likely that the coke was generated from the oligomerization and condensation of the intermediates or byproducts during the isomerization of *endo*-THDCPD. Scheme 1 showed a possible mechanism of coke formation on the HY zeolite for this reaction. The isomerization of *endo*-THDCPD was thought to occur on the Brønsted sites of the HY zeolite via a pentacoordinated carbocation.⁴⁸ The carbenium ion intermediates could further undergo isomerization to generate *exo*-THDCPD or undergo other side reactions such as β -scission and hydrogen transfer to produce various olefin species. Meanwhile, olefin oligomerization reactions catalyzed by acid sites on the HY zeolite could occur as well, leading to the formation of coke.⁴⁹ Under the H₂ atmosphere, the activated H₂ formed on Pt sites contributed to suppress the coking and depress the oligomerization and condensation of coke precursors by hydrogenating the coke precursors. Therefore, it could be concluded that H₂ and Pt played crucial roles in maintaining the catalytic stability of the HY zeolite during the hydroisomerization of *endo*-THDCPD.

4. CONCLUSIONS

By comparing the catalytic stability of the HY zeolite for the liquid-phase isomerization of *endo*-THDCPD into *exo*-THDCPD over a fixed-bed reactor, it was discovered that Pt/HY displayed a longer lifespan for the isomerization process under a H₂ atmosphere. To understand the impact of H₂ and Pt on enhancing the catalytic stability of the HY zeolite, the catalytic performances of HY and Pt/HY under a N₂ or H₂ atmosphere for the isomerization of *endo*-THDCPD were investigated. The results disclosed that the H₂ or N₂ atmosphere had no obvious effect on the catalytic activity

and catalytic stability of the HY zeolite in the reaction, and the *endo*-THDCPD conversion gradually decreased to 60% after 8 h for the HY zeolite in a 0.5 MPa H₂ atmosphere. However, Pt/HY displayed a high catalytic activity and good catalytic stability with 97% *endo*-THDCPD conversion and 96% selectivity for *exo*-THDCPD after 100 h in a 0.5 MPa H₂ atmosphere. The presence of Pt and H₂ could slightly reduce the selectivity of *exo*-THDCPD and promote the selectivity of ring-opening byproducts, which meant that it would not cause huge differences from the expected product distribution. However, the presence of Pt and H₂ could strongly suppress the coke formation on the HY zeolite, enhancing the catalytic stability of the HY zeolite. The mechanism of coke formation was discussed on the basis of coke analysis results. It was indicated that the coke was formed by the oligomerization and condensation of olefin species as coke precursors, which originated from the β -scission reaction or hydride transfer reaction of intermediates during the isomerization process. The H₂ and Pt on Pt/HY were two essential factors to suppress the formation of coke and maintain the performance of HY by means of H₂ activation to hydrogenate the coke precursors. This study provided good potential for designing a new route applied in the hydroisomerization of *endo*-THDCPD to *exo*-THDCPD catalyzed by the Pt/HY zeolite with a long lifespan.

■ AUTHOR INFORMATION

Corresponding Author

Zhiping Tao – Research Institute of Petroleum Processing, Sinopec, Beijing 100083, China; Email: taozp.ripp@sinopec.com

Authors

Wenke Wang – Research Institute of Petroleum Processing, Sinopec, Beijing 100083, China; orcid.org/0000-0002-8662-3123

Jie Zhao – Research Institute of Petroleum Processing, Sinopec, Beijing 100083, China

Dandan Jia – Research Institute of Petroleum Processing, Sinopec, Beijing 100083, China

Zhaolin Fu – Research Institute of Petroleum Processing, Sinopec, Beijing 100083, China

Enhui Xing – Research Institute of Petroleum Processing, Sinopec, Beijing 100083, China; orcid.org/0000-0002-1906-0594

Zhongpeng Zhu – Research Institute of Petroleum Processing, Sinopec, Beijing 100083, China

Rui Yan – Research Institute of Petroleum Processing, Sinopec, Beijing 100083, China

Yibin Luo – Research Institute of Petroleum Processing, Sinopec, Beijing 100083, China; orcid.org/0000-0002-8286-857X

Xingtian Shu – Research Institute of Petroleum Processing, Sinopec, Beijing 100083, China

Complete contact information is available at:
<https://pubs.acs.org/10.1021/acsoomega.1c00212>

Notes

The authors declare no competing financial interest.

ACKNOWLEDGMENTS

This work was supported by the Research Institute of Petroleum Processing, Sinopec.

REFERENCES

- (1) Fort, R. C.; Schleyer, P. V. R. Adamantane: Consequences of the Diamondoid Structure. *Chem. Rev.* **1964**, *64*, 277–300.
- (2) Chenoweth, K.; van Duin, A. C. T.; Dasgupta, S.; Goddard, W. A., III Initiation Mechanisms and Kinetics of Pyrolysis and Combustion of JP-10 Hydrocarbon Jet Fuel. *J. Phys. Chem. A* **2009**, *113*, 1740–1746.
- (3) Zhang, X.; Pan, L.; Wang, L.; Zou, J.-J. Review on synthesis and properties of high-energy-density liquid fuels: hydrocarbons, nano-fluids and energetic ionic liquids. *Chem. Eng. J.* **2018**, *180*, 95–125.
- (4) Cohen, C. A.; Muessig, C. W. Jet and rocket fuel. U.S. Patent 3,381,046 A, 1968.
- (5) Schneider, A.; Ware, R. E.; Janoski, E. J. Isomerization of endo-tetrahydrodicyclopentadiene to a missile fuel diluent. U.S. Patent 4,086,284 A, 1978.
- (6) Chung, H. S.; Chen, C. S. H.; Kremer, R. A. J.; Boulton, R.; Burdette, G. W. Recent Developments in High-Energy Density Liquid Hydrocarbon Fuels. *Energy Fuels* **1999**, *13*, 641–649.
- (7) Khan, A.; Ali, S. S.; Chodimella, V. P.; Farooqui, S. A.; Anand, M.; Sinha, A. K. Catalytic Conversion of Dicyclopentadiene into High Energy Density Fuel: A Brief Review. *Ind. Eng. Chem. Res.* **2021**, *60*, 1977–1988.
- (8) Khan, N.; Abhyankar, A. C.; Nandi, T.; Eswara Prasad, N. Nickel Nanocatalyst Supported Single-Step Hydroconversion of Dicyclopentadiene (DCPD) into High Energy-Density Fuel, Exo-Tetrahydrodicyclopentadiene (Exo-THDCPD). *J. Nanosci. Nanotechnol.* **2019**, *19*, 7982–7992.
- (9) Schleyer, P. v. R.; Donaldson, M. M. Relative Stability of Bridged Hydrocarbons. II. endo- and exo-Trimethylenenorbornane. The Formation of Adamantane_{1,2}. *J. Am. Chem. Soc.* **1960**, *82*, 4645–4651.
- (10) Schleyer, P. v. R. A Simple Preparation of Adamantane. *J. Am. Chem. Soc.* **1957**, *79*, 3292.
- (11) Navrátilová, M.; Sporka, K. Synthesis of adamantane on commercially available zeolitic catalysts. *Appl. Catal., A* **2000**, *203*, 127–132.
- (12) Ji, M.; Zhou, Y.; Luo, Q.; Park, S.-E.; Cai, T. AlCl₃ Supported Catalysts for the Isomerization of Endo-Tetrahydrodicyclopentadiene. *Green Sustainable Chem.* **2013**, *03*, 43–47.
- (13) Wang, L.; Zou, J.-J.; Zhang, X.; Wang, L. Isomerization of tetrahydrodicyclopentadiene using ionic liquid: Green alternative for Jet Propellant-10 and adamantane. *Fuel* **2012**, *91*, 164–169.
- (14) Huang, M.-Y.; Wu, J.-C.; Shieu, F.-S.; Lin, J.-J. Preparation of high energy fuel JP-10 by acidity-adjustable chloroaluminate ionic liquid catalyst. *Fuel* **2011**, *90*, 1012–1017.
- (15) Xing, E.; Mi, Z.; Xin, C.; Wang, L.; Zhang, X. Endo- to exo-isomerization of tetrahydrodicyclopentadiene catalyzed by commercially available zeolites. *J. Mol. Catal. A: Chem.* **2005**, *231*, 161–167.
- (16) Sun, C.-m.; Li, G. Vapor-phase isomerization of endo-tetrahydrodicyclopentadiene to its exo isomer over zeolite catalysts. *Appl. Catal., A* **2011**, *402*, 196–200.
- (17) Li, G.; Hou, B.; Wang, A.; Xin, X.; Cong, Y.; Wang, X.; Li, N.; Zhang, T. Making JP-10 Superfuel Affordable with Lignocellulosic Platform Component. *Angew. Chem., Int. Ed.* **2019**, *58*, 12154–12158.
- (18) Wang, W.; Chen, J.-G.; Song, L.-P.; Liu, Z.-T.; Liu, Z.-W.; Lu, J.; Xiao, J.; Hao, Z. One-Step, Continuous-Flow, Highly Catalytic Hydrogenation–Isomerization of Dicyclopentadiene to exo-Tetrahydrodicyclopentadiene over Ni-Supported Catalysts for the Production of High-Energy-Density Fuel. *Energy Fuels* **2013**, *27*, 6339–6347.
- (19) Guisnet, M.; Magnoux, P. Organic chemistry of coke formation. *Appl. Catal., A* **2001**, *212*, 83–96.
- (20) Guisnet, M.; Costa, L.; Ribeiro, F. R. Prevention of zeolite deactivation by coking. *J. Mol. Catal. A: Chem.* **2009**, *305*, 69–83.
- (21) González, H.; Rodríguez, A.; Cedeño, L.; Ramírez, J.; Aracil, J. Isomerization of C₈ Aromatics over a Pt/Mordenite Catalyst. A Statistical Model. *Ind. Eng. Chem. Res.* **1996**, *35*, 3964–3972.
- (22) Claude, M. C.; Martens, J. A. Monomethyl-Branching of Long n-Alkanes in the Range from Decane to Tetracosane on Pt/H-ZSM-22 Bifunctional Catalyst. *J. Catal.* **2000**, *190*, 39–48.
- (23) Karthikeyan, D.; Lingappan, N.; Sivasankar, B.; Jabarithanam, N. J. Activity and selectivity for hydroisomerisation of n-decane over Ni impregnated Pd/H-mordenite catalysts. *Appl. Catal., A* **2008**, *345*, 18–27.
- (24) Bauer, F.; Ficht, K.; Bertmer, M.; Einicke, W.-D.; Kuchling, T.; Gläser, R. Hydroisomerization of long-chain paraffins over nano-sized bimetallic Pt-Pd/H-beta catalysts. *Catal. Sci. Technol.* **2014**, *4*, 4045–4054.
- (25) Niu, P.; Xi, H.; Ren, J.; Lin, M.; Wang, Q.; Jia, L.; Hou, B.; Li, D. High selectivity for n-dodecane hydroisomerization over highly siliceous ZSM-22 with low Pt loading. *Catal. Sci. Technol.* **2017**, *7*, 5055–5068.
- (26) Wang, W.; Liu, C.-J.; Wu, W. Bifunctional catalysts for the hydroisomerization of n-alkanes: the effects of metal–acid balance and textural structure. *Catal. Sci. Technol.* **2019**, *9*, 4162–4187.
- (27) Wang, L.; Chen, Y.; Jin, S.; Chen, X.; Liang, C. Selective Ring-Shift Isomerization in Hydroconversion of Fluorene over Supported Pt Catalysts. *Energy Fuels* **2016**, *30*, 3403–3412.
- (28) Liu, B.; Chen, F.; Zheng, L.; Ge, J.; Xi, H.; Qian, Y. Synthesis and structural properties of hierarchically structured aluminosilicates with zeolite Y (FAU) frameworks. *RSC Adv.* **2013**, *3*, 15075–15084.
- (29) Ogo, S.; Nishio, T.; Sekine, H.; Onda, A.; Sekine, Y. One pot direct catalytic conversion of cellulose to C₃ and C₄ hydrocarbons using Pt/H-USY zeolite catalyst at low temperature. *Fuel Process. Technol.* **2016**, *141*, 123–129.
- (30) Hengsawad, T.; Srimingkwanchai, C.; Butnark, S.; Resasco, D. E.; Jongpatiwut, S. Effect of Metal–Acid Balance on Hydroprocessed Renewable Jet Fuel Synthesis from Hydrocracking and Hydroisomerization of Biohydrogenated Diesel over Pt-Supported Catalysts. *Ind. Eng. Chem. Res.* **2018**, *57*, 1429–1440.
- (31) Corma, A.; Martínez, A.; Fernandes, L. D.; Monteiro, J. L. F.; Sousa-Aguiar, E. F. Short chain paraffins isomerization on Pt/beta Catalysts. Influence of framework and extraframework zeolite composition. *Stud. Surf. Sci. Catal.* **1995**, *94*, 456–463.
- (32) Xing, E.; Zhang, X.; Wang, L.; Mi, Z. Greener synthesis route for Jet Propellant-10: the utilization of zeolites to replace AlCl₃. *Green Chem.* **2007**, *9*, 589–593.
- (33) Santikunaporn, M.; Herrera, J.; Jongpatiwut, S.; Resasco, D.; Alvarez, W.; Sughrie, E. Ring opening of decalin and tetralin on HY and Pt/HY zeolite catalysts. *J. Catal.* **2004**, *228*, 100–113.
- (34) Kubička, D.; Kumar, N.; Mäki-Arvela, P.; Tiitta, M.; Niemi, V.; Karhu, H.; Salmi, T.; Murzin, D. Y. Ring opening of decalin over

zeolitesII. Activity and selectivity of platinum-modified zeolites. *J. Catal.* **2004**, *227*, 313–327.

(35) Du, H.; Fairbridge, C.; Yang, H.; Ring, Z. The chemistry of selective ring-opening catalysts. *Appl. Catal., A* **2005**, *294*, 1–21.

(36) Almas, Q.; Naeem, M. A.; Baldanza, M. A. S.; Solomon, J.; Kevin, J. C.; Müller, C. R.; Teixeira da Silva, V.; Jones, C. W.; Sievers, C. Transformations of FCC catalysts and carbonaceous deposits during repeated reaction-regeneration cycles. *Catal. Technol.* **2019**, *9*, 6977–6992.

(37) Li, Y.; Zhang, C.; Liu, Y.; Tang, S.; Chen, G.; Zhang, R.; Tang, X. Coke formation on the surface of Ni/HZSM-5 and Ni-Cu/HZSM-5 catalysts during bio-oil hydrodeoxygenation. *Fuel* **2017**, *189*, 23–31.

(38) Zhang, Y.; Li, M.; Xing, E.; Luo, Y.; Shu, X. Coke evolution on mesoporous ZSM-5 during methanol to propylene reaction. *Catal. Commun.* **2019**, *119*, 67–70.

(39) Magnoux, P.; Roger, P.; Canaff, C.; Fouche, V.; Gnep, N. S.; Guisnet, M. New Technique for the Characterization of Carbonaceous Compounds Responsible for Zeolite Deactivation. *Stud. Surf. Sci. Catal.* **1987**, *34*, 317–330.

(40) Mckenna, A. M.; Blakney, G. T.; Xian, F.; Glaser, P. B.; Rodgers, R. P.; Marshall, A. G. Heavy Petroleum Composition. 2. Progression of the Boduszynski Model to the Limit of Distillation by Ultrahigh-Resolution FT-ICR Mass Spectrometry. *Energy Fuels* **2010**, *24*, 2939–2946.

(41) Liu, H.; Mu, J.; Wang, Z.; Ji, S.; Shi, Q.; Guo, A.; Chen, K.; Lu, J. Characterization of Vanadyl and Nickel Porphyrins Enriched from Heavy Residues by Positive-Ion Electrospray Ionization FT-ICR Mass Spectrometry. *Energy Fuels* **2015**, *29*, 4803–4813.

(42) Xing, E.; Zhang, X.; Wang, L.; Mi, Z. Molecular dimensions of tetrahydrodicyclopentadiene isomers and shape selectivity of zeolitic catalysts. *Catal. Commun.* **2005**, *6*, 737–741.

(43) Kwak, K.-Y.; Kim, M.-S.; Lee, D.-W.; Cho, Y.-H.; Han, J.; Kwon, T. S.; Lee, K.-Y. Synthesis of cyclopentadiene trimer (tricyclopentadiene) over zeolites and Al-MCM-41: The effects of pore size and acidity. *Fuel* **2014**, *137*, 230–236.

(44) Fouche, V.; Magnoux, P.; Guisnet, M. Coking, ageing and regeneration of zeolites: XI. Coke formation and deactivation of Pt-ultrastable zeolite HY and Pt/H-mordenite catalysts during hydrogenation of benzene. *Appl. Catal., B* **1990**, *58*, 189–198.

(45) Santikunaporn, M.; Alvarez, W. E.; Resasco, D. E. Ring contraction and selective ring opening of naphthenic molecules for octane number improvement. *Appl. Catal., A* **2007**, *325*, 175–187.

(46) Iglesia, E.; Soled, S. L.; Kramer, G. M. Isomerization of Alkanes on Sulfated Zirconia: Promotion by Pt and by Adamantyl Hydride Transfer Species. *J. Catal.* **1993**, *144*, 238–253.

(47) Moleró, H.; Bartlett, B. F.; Tysoe, W. T. The hydrogenation of Acetylene Catalyzed by Palladium: Hydrogen Pressure Dependence. *J. Catal.* **1999**, *181*, 49–56.

(48) Lau, G. C.; Maier, W. F. Polycyclic hydrocarbon rearrangements in zeolites. A mechanistic study. *Langmuir* **1987**, *3*, 164–173.

(49) Pater, J. P. G.; Jacobs, P. A.; Martens, J. A. 1-Hexene Oligomerization in Liquid, Vapor, and Supercritical Phases over Beidellite and Ultrastable Y Zeolite Catalysts. *J. Catal.* **1998**, *179*, 477–482.